Thanks to the reviewers we were able to greatly improve this manuscript and we could hopefully answer all comments made good enough. It was quite a lot of work we put into this manuscript after receiving the reviews and a big part of it was completely rewritten or changed and quoting it all here in the answer letter would make it hard to follow. Therefore, I will just briefly explain the biggest changes made here and kindly refer to the new manuscript.

We completely rewrote the mathematical description of the model which now includes the dimensional equations and a small chapter about how these equations are solved. We also use a new non-dimensionalization using the Stokes velocity and the radius of the initial perturbation. This allows us now to describe the Stokes limit, where the old description failed. It might also help to better understand the quite complex model setup. Due to the change in scaling all figures had to be remade and are now hopefully up to the standards and everything is readable.

Regarding the figures, we removed former figure 3 as we think that it didn't give much more information than figure 2 already gave and is quite complicated to understand and describe. Instead we added a new figure containing a resolution test which is described and analyzed in a new chapter called "numerical issues".

The main point in this new manuscript is that we now state that the focusing, we formerly stated are small porosity waves, are channels that build up in front of the wave due to the horizontal stresses occurring there. This new statement is described and analyzed in the results part of the manuscript, where it replaces the argument of the small porosity waves.

In the discussion we now discuss the growth rates of these channels in our models and compare them to Stevenson (1989).

Several other parts in the manuscript had to be changed according to our new statement and are not especially mentioned here but are marked in the updated manuscript in red.

Below you will find the comments made by the reviewers in black and our answers in red.

Anonymous Referee #1

Received and published: 6 August 2020

The submitted manuscript presents parametric study of porosity wave propagation in viscous porous rocks. The novel aspect of the manuscript is the investigation of the effect of compaction length on the evolution of rising porosity waves. This is a welcome contribution since influence of material parameters and the size/geometry of the source region remains unclear. However, paper has several major drawbacks that need to be addressed.

Authors claim that they consider transition from porosity waves to diapirism. Here, I see a major conceptual problem. As often in geosciences, different terms got confused and mixed up. As I could grasp from the text, by diapirs authors understand wide structures, while porosity waves are assumed to be narrow structures. This is already in contradiction with e.g. Wikipedia's definition of diapir, which reads as "A diapir,. . . is a type of geologic intrusion in which a more mobile and ductily deformable material is forced into brittle overlying rocks. Depending on the tectonic environment, diapirs can range from idealized mushroom-shaped Rayleight-Taylor-instability-type structures in regions with low tectonic stress such as in the Gulf of Mexico to narrow dykes of material that move along tectonically induced fractures in surrounding rock." Thus, according to Wikipedia all structures produced by the authors would fall into diapir category.

We do not agree with the English version of Wikipedia. Diapirism is not necessarily related to brittle overburden and to a more mobile buoyant material. We use diapirism in the sense it had been defined and introduced e.g. by Turcotte and Schubert (1981), Simpson, 1989, and many others in the 1970s and 1980s. We specify our (and the common geologic) definition:

"Addressing different melt ascent mechanisms it may be useful to specify our definition of diapirism. Originating from the Greek "*diapeirein*", i.e. "to pierce through", diapirism describes the "buoyant upwelling of relatively light rock" (Turcotte and Schubert, 1981) through and into a denser overburden. In the general definition the rheology of the diapir and ambient material is not specified, both can be ductile as in our case, but often, the overburden is assumed being more viscous or even brittle. Buoyancy may be of compositional or phase related origin, e.g. due to the presence of non-segregating partial melt (Wilson, 1989). Based on these definitions in our case a diapir is a rising, partially molten body or porosity anomaly with zero fluid-solid separation velocity. Mathematically the equations of motion of the two-phase system degenerate to the Stokes equation (see below)."

In the introduction authors describe diapirs as structures that are formed by RayleighTaylor instability, which is commonly considered to be due to interaction of two immiscible fluids, whose behavior is described by Navier-Stokes equations. Porosity wave instability is described by Darcy law in combination with Navier-Stokes for solid. In other words, these are two different systems of equations. However, authors solve only porosity wave system of equations and thus Rayleigh-Taylor instability is not even considered in the paper. This is all very confusing for the reader and needs sharpening of the introduction and model description section. I would even suggest changing the title as diapirs in the sense of Rayleigh-Taylor instability are not even considered in the manuscript. I would suggest something more to the point, like "The effect of compaction length on solitary porosity waves and its implications for magma ascent mechanisms".

We do not consider or mention Rayleigh Taylor instability in our paper, per definition a RT instability starts from a stratified and not from a buoyant circular anomaly. But thanks to the reviewer, we specify the Darcy and Stokes type of equations for the both end member now.

Another problem of the paper is the reliability of the presented simulation results. When changing the compaction length, authors produce porosity waves of different radius. Eventually, they become very narrow. We know from previously published research that numerical codes treating porosity waves are very sensitive to the resolution, so that several grid points are required for accurate results [Rass et al., 2019]. Thus, convergence of numerical results at higher resolution needs to be checked before acceptance of the paper. This is especially important for r'>10. We see from results presented in the first row of Figure 1 (low values of r') that porosity waves are circular blobs as expected. Other results exhibit some tails below the circular wave that authors interpret as flow focusing. However, these are exactly the results that may suffer from lack of resolution. Besides, tails behind the major porosity wave were repeatedly reported from 1D and 2D numerical models [Connolly and Podladchikov, 1998; 2000; Rass et al., 2019]. These disappear when simulations are left for longer time periods and waves and allowed to propagate further from the source region. I expect that if authors will allow their waves to run longer, they will see that eventually perfectly circle blobs detach from the cloud. Thus, observed pattern is not a flow focusing as such but just an initial smearing of the fluid propagation front. Eventually secondary waves could form from the remaining cloud.

Yes, numerical resolution is a major problem in modelling porosity waves and or model setup will inevitably lack in decent compaction length resolution. Anyways, we now state that the peaks we observe in the transitional regime are channels which are still resolvable with our resolution. Channels also explain why the tail behind the leading wave does not get smaller or even vanish but growth with time. We now calculate growth rates and show that they agree with Stevenson (1989).

Still, resolution is a major issue and we added a new chapter about “numerical issues”.

Some detailed comments:

Section 2.1. The described above possible confusion with terminology requires extra care when describing your governing equations. You really need to explain what the similarities and differences in the description of both instabilities are and what exactly is included into your equations. Please describe here underlying assumptions of the model of Dohmen et al. What kind of simplifications assumed in this model? I think that a very brief approach of referring to Dohmen et al. is inappropriate here.

Now we specify how the former equ 11 is derived, which reveals the inherent assumptions. As for the “small fluid viscosity limit” we add:

“In the small fluid viscosity limit the viscous stresses within the fluid phase are neglected, resulting in a viscous stress tensor in the Stokes equation of the mixture (equ. 4), in which only the stresses in the solid phase are relevant. This is evident from the definition of the viscous stress tensor, which only contains matrix and not fluid viscosities. Melt viscosities of carbonatitic, basaltic or silicic wet or dry melts span a range from < 1 Pa s to extreme values up to 10^{14} Pa s (see the discussion in Schmeling et al., 2019), while effective viscosities of mafic or silicic partially molten rocks may range between 10^{20} Pa s and 10^{16} Pa s, depending on melt fraction, stress, and composition. Thus, in most circumstances the small fluid viscosity limit is justified.”

Lines 50-55. List of principal notations would help the reader, given that you have a lot of quantities with complicated indexes, such as δc0. Why not just δ? Why Darcy velocity has complicated index vsc0, why not just vD? Why permeability has index kφ and not just k? Are you using k for something else? Please consider carefully, how to make notations simpler. Equation 5. It is a bit odd to see ρs as an independent scale here together with 3 other scales (for length, velocity and viscosity). In principle, you can have only 3 independent scales in this problem. When you use them, you'll just get some non-dimensional parameters such as sedimentation rate in your system of equations.

As we completely revised our mathematical description, this problem is hopefully solved. We still stick to k_φ and δ_c as these notations are commonly used but we got rid of the zero notations.

Line 73. Please discuss small fluid viscosity limit. What are the typical viscosity values for solid magmatic rocks and for melt? What effects your simplified equations ignore? Equation 11. Please comment here whether eqn (11) is a consequence of a usual Darcy equation or it follows some other governing law, e.g. Navier-Stokes? Which terms are omitted/presented?

See above.

Lines 85 - 90. You do not vary the radius of anomaly. The radius of your anomaly has always the same size. In the non-dimensional world, it is always w'=0.05L'. In the dimensional world it is always w=0.05L. What you are really looking at is the effect of lighter/heavier fluid in a more/less permeable rock, which will naturally have porosity waves of different size The description given in this para is very confusing.

This was probably also caused due to the confusion with the non-dimensionalization. But we are in fact changing the radius of the emerging solitary wave. When we double the characteristic compaction length of the model the solitary wave will be also double the size in [m] as the wave will be the same size in terms of compaction length.

Now with the new description it might be easier to understand the model setup. We also gave a small example.

Lines 90-91. Please comment how many grid points you have for the thinnest porosity wave.

As we now state that they are channels and not porosity waves the number of grid points per wave is no longer that important, but we also have a look at the resolution with a new figure with different resolutions. We see that the channels are resolvable as long as the grid size is approximately in the order of the compaction length.

Equation 14. Please explain this equation or provide reference for it.

This equation is the commonly used Stokes equation, which is now referenced with (Turcotte & Schubert, 1981).

Line 102. "As this radius and the maximum melt fraction change strongly during the run of a model" This just indicates that you did not reach steady-state wave propagation. See comment above.

See above.

Lines 105-107. I do not understand what you are trying to say here.

Yes, this sentence was a bit odd and is no longer part of the new mathematical description.

Section 3.1. This definition is very arbitrary. You do not have any diapirs in your model. You only have porosity waves of varying width. As we know, the speed of porosity wave depends on it size and thus you would have bigger and smaller waves travelling with different speed. It is interesting to compare those to the speed of diapirs, but they do not become diapirs here.

This might be a confusion due to the old description of the theory, as it wasn't able to describe the Stokes limit. With the new description we now are able to describe it and it might be now clear that we get diapirs in the sense we stated above.

Line 109. "The transition from porosity wave to diapirism: Varying the initial wave radius" You do not vary initial wave radius, only compaction length, which is different.

See above.

Line 114. It is too early to talk about focusing at this depth. Your waves will become circular when they will propagate higher.

Now with the channels we clearly observe focusing in the sense that melt gets accumulated in a smaller horizontal area.

Lines 115-125. Porosity waves are very sensitive to resolution. How many grid points do you have per porosity wave for your runs at r'>=20? All discussions for these runs are meaningless as you clearly run into a problem of not resolving a physical process properly. For all figures with r'>=20 you need to show convergence at higher resolution.

See above.

Lines 128-134. What is the point of giving analytical cases that do not correspond your simulations? You have only n=3 and m=1. All these extra cases and lines only confuse reader without much useful information.

The figure has been revised and now shows just the relevant case of n=3 and m=1.

Line 133. Again, here I see a big issue with terminology and conceptual understanding. You do not have diapirs. Porosity within your model is never higher than 6 times the background, which is 0.5

See above.

Lines 170-175. I do not see how this is relevant for your simulations and porosity waves. It is precisely the difference in solid and fluid densities that drives evolution of porosity waves.

This is part of our Boussinesq approximation, where all density differences are dropped but in the buoyancy term of the momentum equations.

We now describe this approximation in our mathematical description.

Line 233. "This could lead to the propagation of magma-filled cracks" Again, remember that max porosity in your simulations is 3

Yes, this is true, but the melt porosities would be way higher if we would allow for further focusing. Also our model starts with very low melt porosities as these models are more robust, but we would observe the same behavior for higher porosities.

Lines 235-236. "But this effect might not be strong enough to lead" Which effect? Considered in your manuscript or in the paper of Connolly and Podladchikov? Unclear sentence.

The sentence has been changed to:

"But this upward weakening might not be strong enough to lead to the focusing needed for the nucleation of dykes"

Lines 238-239. Did you perform simulations with varying porosity/permeability or is this a hypothetical scenario you are describing? Please refer to simulations with varying/layered media.

We did some simple tests with several different layers that have different shear and bulk viscosities and solitary waves passing through them as port of another project. This test was just very simple and not enough to show in this paper but shows exactly what we describe here, a focusing. We did not, however, perform simulations with varying background porosity as this model setup might be even more complex. The case of differing viscosity should however have the same effect, as it also changes the compaction length.

The sentence has been changed to:

"In the hypothetic case of a porosity wave reaching the top of a magma chamber, the background porosity might decrease which would most certainly lead to focusing, because the compaction length will decrease, and eventually, when reaching melt free rocks, the melt rich fingers may stall as in our models at $r > 50 \cdot \delta_c$ and the rising melt will accumulate and enter the pure diapirism regime"

Figure 2. Explain whether the colored lined are obtained from your numerical simulations or equations (14) - (15). You also need to provide somewhere equation used for dashed lines and comment on the parameters used in this equation.

The dashed lines in the original figure are now the colored ones. They are calculated semi-analytically using the program provided by Simpson & Spiegelman (2011) and there is therefore no analytical equation to describe these curves.

The former colored lines were calculated analytically with the mentioned equation for the Stokes sphere, but this information is now no longer needed.

The caption of the figure was changed to:

The dashed line marks the velocity of the Stokes sphere ($v' = 1$). The colored lines show the velocity of a 2D solitary wave, calculated semi-analytically by Simpson & Spiegelman (2011), in our non-dimensionalization, based on the radii shown in the legend.

Figure 3. It is a very interesting idea to compare Stokes and porosity wave velocities. This is one of the central points of this study and therefore much more careful description is needed here. Which equations and which parameters did you use for both? What is the sensitivity of these equations to parameters that are kept fixed (e.g., n or φ0, etc). Obviously, your model did not reproduce any of the analytical velocities. Given the issue of resolution described above, you need to confirm your results at higher resolution. Letters on this figure and figure 4 are unreadable. Please increase the font.

We now got rid of figure 3 as it was quite complex and did not really give any more information that is not already in figure 2. Sensitivity to the parameters kept fixed is a whole different story. Changing φ_0 should lead to minor changes in the results as we used simplified viscosities. In Dohmen et al. (2019) we have a look at the behavior of SWs for different background porosities. They play a major roll with the more complex, lower viscosities, used there. Changing *n* would probably change the results, but it would need much more time to get a similar work with n=2.

References:

Connolly, J. A. D., and Y. Y. Podladchikov (1998), Compaction-driven fluid flow in viscoelastic rock, Geodin Acta, 11(2-3), 55-84, doi:Doi 10.1016/S0985-3111(98)80006-5.

Connolly, J. A. D., and Y. Y. Podladchikov (2000), Temperature-dependent viscoelastic compaction and compartmentalization in sedimentary basins, Tectonophysics, 324(3), 137-168.

Rass, L., T. Duretz, and Y. Y. Podladchikov (2019), Resolving hydromechanical coupling in two and three dimensions: spontaneous channelling of porous fluids owing to decompaction weakening, Geophys J Int, 218(3), 1591-1616, doi:10.1093/gji/ggz239.

Anonymous Referee #2

General comments

The submitted manuscript systematically investigates magma ascent dynamics in order to capture the transition from the solitary wave regime to diapirism. The authors explore this transition by varying the relative compaction length of the system - here by changing the model extend dimensions while keeping the compaction length constant. Investigating fluid transport mechanisms in Earth subsurface is of broad interest with applications not only limited to melt in the crust, and thus the study is a welcome contribution. Although the title and abstract sound promising, the study presents several important issues that need to be addressed before to be further considered for publication.

1. The study's design

The authors claim to resolve the transition from solitary wave of porosity to Stokes-like diapiric rise of magma. These two regimes are very different. The solitary waves of porosity occur in two-phase medium, when the fluid has a relative velocity compared to the solid. The diapiric ascent occurs if the fluid has no or very limited mobility with respect to the solid and thus the medium behaves as single-phase. The authors report here briefly the two-phase flow equations they rely on, which permit to resolve the two-phase motion. However, it is unclear what happens in the single-phase flow limit. In this limit, the equations should reduce to the single phase (Navier-) Stokes system. This part is totally absent from the study, both in the physical description (system of equations) and from the numerical implementation. The authors overlooked a study from Scott (1988) investigating a very similar research question, namely "The competition between percolation and circulation in a deformable

porous medium". This short communication may be highly relevant and may support or challenge some statement claimed by the authors.

We totally agree with the reviewer here. The equations given in the former version describe the two-phase flow limit but fail in the Stokes limit. Because of that we introduced a new non-dimensionalization that is capable of describing both limits.

The “Governing equations” section was completely rewritten.

We now mention the research of Scott (1988):

This switch from negative to positive mass flux was already observed by Scott (1988), but while he changed the viscosity ratio, we change the radius and keep the viscosity ratio constant. Both describe the transition from a two-phase limit towards the Stokes limit, but in our formulation we are able to reach the Stokes limit while Scott (1988) is still in the two-phase flow regime.

2. The numerical implementation

In this study, the authors rely on numerical modelling to investigates the effect of changes in compaction length, or rather vary the domain size keeping the compaction length fixed. Being a numerical study, the current manuscript seriously lacks in robust model description, numerical implementation, benchmarking. These (non-exhaustive) steps are the basic technicalities one is expected to report when performing numerical experiments. The authors emphasise both in the Abstract and the Introduction the numerical challenges relative to accurately resolving fluid migration in the subsurface. However, no further discussion about numerical method, implementation, benchmarking, sensitivity analysis, etc... is present in the manuscript. The model configuration is poorly described and some basic information such as the numerical grid resolution should be reported in a well-crafted "Numerical Implementation" section well before the final discussion. Although focus should not be on benchmarking, ensuring accuracy of the numerical scheme and related results is primordial in studies like this one. As reported recently by Räss et al. (2019), lack of numerical resolution may lead to erroneous results. I am afraid that part of the results reported in this study are under-resolved, as at least a few tens of gridpoints are needed per compaction length to obtain accurate results. Also missing is the description of the transition from two-phase flow to single-phase flow. How do the authors treat the very small compaction length limit? In this limit, Stokes flow is dominating, and the motion of the fluid pocket needs advection of the solid matrix. There is no information regarding this important point in the manuscript. The governing equations are very cryptic, and it would be very helpful to see the finally implemented closed system of equations that is actually solved numerically, together with information on the numerical scheme that is used.

Yes, the numerical resolution is a major issue, but now, as we revised our statements, the resolution is no longer as big of a problem as before. The small porosity waves we observed in the transition regime would have been most certainly not decently resolve, but now we state that we observe channeling in this regime, based on Stevenson (1989), which are resolvable by our resolution. The channel’s wavelength in our models is in the same order as in Stevenson (1989) and the growth rate is explainable as well.

We still added a small chapter about numerical issues to the results, that tells a little bit about the issues observed.

We also give a small introduction on how we solve the equations numerically and, as already stated above, we changed the mathematical description so that we are now able to reach the Stokes Limit.

3. The quality of the reported results

The reported results are interesting but in light of the previous comments, further work would be welcome to refine the Results and Discussion sections. The authors could put some additional efforts in crafting better quality figures. There are missing labels, fonts are very small and hardly readable in some cases, and figure captions display repetitions and miss important details. Also, it may be interesting to report in form of quiver plots the solid and fluid velocity components as those could be directly compared to results obtained by Scott in 1988.

All figures were revised and are now hopefully up to the standards.

To summarise, this manuscript tackles an interesting and not yet fully resolved question, but the study's design, numerical implementation and overall quality should be seriously improved before being considered for publication. Addressing these issues are important as in the current status it is hard for the reader to discriminate between resolved dynamics or numerical artefacts, especially in the transition regime. In the Discussion, the authors provide some insights in the challenges related to resolving the two-phase dynamics for large domains (or small compaction length). There may be a conceptual study design issue there. The authors spell out all the pitfall and they don't, but their study actually reports results that exactly suffer from those drawbacks. and may not be accurate. A potential way to improve the study would be to move a large part of the issues raised in the discussion to the Section 2. For example, the discussion about the numerical grid resolution should appear much earlier. Then, one could discuss the issue, try to solve it. And if results cannot be trusted, then one should identify them and discard them from the analysis.

Detailed comments

l.18: In the current status, these may be numerical artefacts as well. Appropriate benchmarking would be welcome (e.g. running a test setup at various resolutions and reporting the results).

We now state that the "numerical artefacts" mentioned are channels which are resolvable and show its dependence of resolution in a resolution test.

l.21: For accurate results of porosity waves, numerical resolution should always be such to have about 10 grid points per compaction length.

Yes, such a resolution would be desirable, but is hard to reach in many models. Anyways, as we now state channels this minimum resolution criteria is no longer applicable.

l.23-24: True, one should be careful. Please report how you carefully addressed these resolution issues.

See above.

l.47-49: Important question on "what are the numerical implications on modelling magma transport". Within the manuscript, however, these implications are discussed but it appears that the suggestions provided are not followed by the authors themselves.

See above.

Section Introduction: Please update it putting your contribution in light of previous work such as Scott (1988) and other potential studies.

We added a small comparison of our models to Scott (1988):

"Scott (1988) already had a look at a similar scenario. He calculated porosity waves changing the compaction length by altering the shear to bulk viscosity ratio, while we want to change the radius of a partially molten perturbation in terms of compaction lengths but keeping the viscosity constant.

While Scott (1988) was not able to reach the single-phase flow endmember due to his setup we can reach this endmember with our description and can show how the transition looks like."

eq.8-11: These are non-intuitive formulation of the momentum balance. What do v_1 and v_2 stand for? Please take some place to better describe the approach.

We completely revised the mathematical description and now explain how we get the momentum balance. This description is hopefully more intuitive. v_1 and v_2 have been explained as well.

Section 2.2: Please complete the model setup.

With the new non-dimensionalization the model setup is hopefully better understandable. We also give a small example as the model series is not really intuitive.

l.85: What value of A do you use in the experiments?

We now mention the Amplitude of the wave:

" … where A is the amplitude equal to 0.03 in our models…"

l.90: This may be problematic as number of grid points per compaction length will decrease with increased nondimensional box size.

Yes, this is a problem, even though we now observe channels. But it is not really possible to keep the resolution of the compaction length constant. From r'=1.5 to r'=100 we would have to increase the resolution with a factor of 66, corresponding to a resolution of 13201x13201. Even when we say we don't need a higher resolution for the bigger radii as the compaction length doesn't need to be resolved as good, we still have very high resolutions with high CPU-times. We also observed that some models become unstable with very high resolutions, which is not explainable by now.

l.92: Can you precise what out and inflow conditions you use for the solid? Majority two-phase flow simulation apply free slip boundary conditions for the solid or porous matrix. Please clarify the model configuration - this is crucial for reproducible science.

We now describe the in and outflow more:

"At the top and the bottom, we prescribe an out- and inflow for both melt and solid, respectively, which is calculated analytically for the background porosity. This is necessary because we have a background melt fraction φ_0, that has a certain buoyancy which would lead to an accumulation of melt at the top of the model. We therefore calculate the segregation velocity for background porosity using equation (17) without the viscous stress term. The corresponding matrix velocity is calculated using the conservation of mass."

l.93: What do mirroring boundary conditions refer to?

We now explain the mirroring boundary conditions:

"At the sides we use mirroring boundary conditions, which corresponds to a symmetry axis, where no horizontal flow is allowed."

l.98 + eq.14: Please provide relevant reference for the Stokes velocity?

The Stokes velocity is now introduced earlier in the mathematical description and a reference has been added: Turcotte & Schubert (1982).

l.99: Please justify the choice of the radius you utilise in the Stokes formula.

We added a small justification:

"We use the halfwidth of the initial perturbation as radius for the Stokes velocity. This is reasonable as the amount of melt in the perturbation is approximately equal to the amount of melt in a spheres cut with a sharp boundary of radius r, for what the Stokes equation is valid."

eq.15: Ar not defined

Ar was actually A times r, where A is the amplitude of the initial perturbation and r its radius. With the new description A has been replaced by φ_{max}.

Section 2: Besides the model setup, please report what final equations are implemented in the numerical model. Please also report about your numerical implementation, discretisation, solution strategy; all standard components one is expected to see in a numerical study that would enable reproducible science.

The new mathematical description might now solve this comment, as we now start with the dimensional equations. We also added a paragraph to the numerical strategy.

l.117: This may indeed show lack of numerical resolution.

See above.

l.121-126: No focussing is expected for linear shear and bulk rheology. The focussing you report here may rather be attributed to the still transient state of the model evolution - maybe due to the coarse resolution. To verify this, a higher resolution simulation on a larger domain should be carried out and running until the shape stabilises.

We now state that this focusing is a channel which is able to evolve with the rheology used in this work.

l.128-132: Why to report various analytical values when your simulation was carried out only with n=3, m=1. This only confuses the reader.

Good point. With the revision of the figures we now show just the n=3, m=1 case. With the new depiction it would have been even more confusing.

l.164.167: Internal circulation would be great to see in a figure. It is difficult to assess and acknowledge your findings based on text only.

As this chapter was deleted, we don't mention the internal circulation. Just for interest one could add a vector field to one of the figures, but the waves shown are all to small to see something then. Adding a new figure wouldn't make much sense as it wouldn't be referred to.

l.170-171: How can you neglect the density difference between solid and melt. This should be the driving force.

We neglect the density difference everywhere but in the buoyancy terms of the momentum equations. This is part of the Boussinesq approximation, we now explain in the mathematical description.

l.218: This conclusion should be verified by a higher resolution run.

See above.

Section 3: May need further development upon updated results

The section was partly rewritten and now addresses some of the issues stated above.

l.224-248: Interesting insight but all these hypotheses should be tested within appropriate modelling framework including spatial variations in the suggested material parameter fields and using sufficient numerical grid resolution to allow resolving the smallest features. Also, note that focussing will only occur if there is asymmetry among compaction and decompaction of the porous matrix, i.e. for non-linear rheology.

We now replaced focusing with channeling which is able to evolve with linear rheology. Still we are not able to resolve even the smallest features but the channeling we now state is less affected by the lack of numerical resolution.

l.249-264: Good point, but it seems that this study exactly shows the reported artefacts in the results.

See above.

References

Scott, D. R. (1988). The competition between percolation and circulation in a deformable porous medium. Journal of Geophysical Research: Solid Earth, 93(B6), 6451-6462.

Räss, L., Duretz, T., & Podladchikov, Y. Y. (2019). Resolving hydromechanical coupling in two and three dimensions: spontaneous channelling of porous fluids owing to decompaction weakening. Geophysical Journal International, 218(3), 1591-1616

Magma ascent mechanisms in the transition regime from solitary porosity waves to diapirism

Janik Dohmen[1], Harro Schmeling[1]

[1]Institute for Geoscience, Goethe University, Frankfurt, Germany

Correspondence to: dohmen@geophysik.uni-frankfurt.de

Abstract

In partially molten regions inside the earth melt buoyancy may trigger upwelling of both solid and fluid phases, i.e. diapirism. If the melt is allowed to move separately with respect to the matrix, melt perturbations may evolve into solitary porosity waves. While diapirs may form on a wide range of scales, porosity waves are restricted to sizes of a few times the compaction length. Thus, the size of a partially molten perturbation controls whether a diapir or a porosity wave will emerge. We study the transition from diapiric rise to solitary porosity waves by solving the two-phase flow equations of conservation of mass and momentum in 2D with porosity dependent matrix viscosity. We systematically vary the initial size of a porosity perturbation from 1.5 to 100 times the compaction length. If the perturbation is much larger than a regular solitary wave, its Stokes velocity is large and therefore faster than the segregating melt. Consequently, the fluid is not able to form a porosity wave and a diapir emerges. For small perturbations solitary waves emerge, either with a positive or negative vertical matrix velocity inside. In between the diapir and solitary wave regimes we observe a third regime of porosity wave or diapir

induced melt focusing and channeling. In these cases, diapirism is dominant but the fluid is still fast enough to locally build up channels and rise in front of the bigger perturbation. These channels have a scale of the order of a few compaction lengths and evolve as long as this length scale is decently resolved. We assume, based on resolution tests, that channels will also build up in the diapir regime with higher resolution.

1 Introduction

In many scenarios inside the earth the process of a fluid moving relatively to a viscously deformable porous matrix is an important transport mechanism. The physics of these scenarios were firstly described by McKenzie (1984) and it was later shown by several authors that these equations allow for the emergence of solitary porosity waves (Scott & Stevenson, 1984; Barcilon & Lovera 1989; Wiggins & Spiegelman, 1995). Porosity waves are regions of localized excess fluid that ascend with permanent shape and constant velocity, controlled by compaction and decompaction of the surrounding matrix.

Even though these porosity waves were of vast interest for many authors over the last decades and the possible consequences on geochemistry and fluid flow in lower and middle crust in general (e.g. Watson & Spiegelman, 1994; McKenzie, 1984; Connolly, 1997; Connolly & Podladchikov, 2013, Jordan et al., 2018, Richard et al., 2012) or the effects of matrix rheology on porosity waves (e.g. Connolly & Podladchikov, 1998; Yarushina et al., 2015; Connolly & Podladchikov, 2015; Omlin et al., 2017; Dohmen et al., 2019) have been examined, there are still open questions. One open question is that of the scaling. The size of a solitary porosity wave is usually of the order of a few compaction lengths (McKenzie, 1984; Scott & Stevenson, 1984; Simpson & Spiegelman, 2011), but this length scale varies over a few orders of magnitude, depending on the shear and bulk viscosity of the matrix, fluid viscosity and permeability (see 1) with typical values of 100-10000 meters (McKenzie, 1984; Spiegelman, 1993).

On the other hand, partially molten regions in the lower crust or upper mantle are prone to gravitational instabilities such as Rayleigh-Taylor instabilities or diapirism (e.g. Griffith, 1986; Bittner and Schmeling, 1995; Schmeling et al., 2019). As characteristic wavelengths of Rayleigh-Taylor instabilities may be similar, but also of significantly different order of those of porosity waves, the question arises how these two mechanisms interact and how does the transition between magmatic rise due to diapirism or porosity wave look like. Scott (1988) already had a look at a similar scenario. He calculated porosity waves changing the compaction length by altering the shear to bulk viscosity ratio, while we want to change the radius of a partially molten perturbation in terms of compaction lengths but keeping the viscosity the same. While Scott (1988) was not able to reach the single-phase flow endmember due to his setup we can reach this endmember with our description and can show how the transition looks like.

The extent of partially molten scenarios inside the earth's mantle vary over many orders of magnitude and this transition might have an important effect on the evolution of these regions. In this work we

want to address this problem and look especially on what happens for different sizes of initial perturbations and what are the numerical implications on modelling magma transport.

Addressing different melt ascent mechanisms, it may be useful to specify our definition of diapirism. Originating from the Greek "*diapeirein"*, i.e. "to pierce through", diapirism describes the "buoyant upwelling of relatively light rock" (Turcotte & Schubert, 1982) through and into a denser overburden. In the general definition the rheology of the diapir and ambient material is not specified, both can be ductile as in our case, but often, the overburden is assumed being more viscous or even brittle. Buoyancy may be of compositional or phase related origin, e.g. due to the presence of non-segregating partial melt (Wilson, 1989). Based on these definitions in our case a diapir is a rising, partially molten body or porosity anomaly with zero fluid-solid separation velocity. Mathematically the equations of motion of the two-phase system degenerate to the Stokes equation (see below).

2 Theoretical Approach

2.1 Governing equations

The formulation of the governing equations for the melt-in-solid two-phase flow dynamics is based on McKenzie (1984), Spiegelman & McKenzie (1987) and Schmeling (2000) assuming an infinite Prandtl number, a low fluid viscosity w.r.t. the effective matrix viscosity, zero surface tension, and the Boussinesq approximation. In the present formulation the Boussinesq approximation (BA) assumes the same constant density for the solid and fluid except for the buoyancy terms of the momentum equations for the solid and fluid. In the following all variables associated with the fluid (melt) have the subscript f and those associated with the solid have the subscript s. Applying the BA the equation for the conservation of the mass of the melt is

$$\frac{\partial \varphi}{\partial t} + \vec{\nabla} \cdot \left(\varphi \vec{v}_f\right) = 0, \tag{1}$$

and the mass conservation of the solid is

$$\frac{\partial (1-\varphi)}{\partial t} + \vec{\nabla} \cdot ((1-\varphi)\vec{v}_s) = 0. \tag{2}$$

φ is the volumetric rock porosity (often called melt fraction), $\vec{v}_f$ and $\vec{v}_s$ are the fluid and solid velocities, respectively. The momentum equations are given as a generalized Darcy equation for the fluid separation flow

$$\vec{v}_f - \vec{v}_s = -\frac{k_\varphi}{\eta_f \varphi}\left(\vec{\nabla} P - \rho_f \vec{g}\right), \tag{3}$$

where ρ_f is the fluid density, and the Stokes equation for the mixture

$$\rho \vec{g} - \vec{\nabla} P + \frac{\partial \tau_{ij}}{\partial x_j} = 0. \tag{4}$$

k_φ is the permeability that depends on the rock porosity

$$k_\varphi = k_0 \varphi^n, \tag{5}$$

η_f is the melt dynamic viscosity, $\vec{g}$ is the gravitational acceleration, ρ is the density of the melt – solid mixture, P is the fluid pressure (including the lithostatic pressure), whose gradient is driving the motion, and τ_{ij} is the viscous stress tensor

$$\tau_{ij} = \eta_s \left(\frac{\partial v_{si}}{\partial x_j} + \frac{\partial v_{sj}}{\partial x_i} \right) + \left(\eta_b - \frac{2}{3}\eta_s \right) \delta_{ij} \nabla \cdot \vec{v}_s. \tag{6}$$

η_b is the bulk viscosity. The linearized equation of state for the mixture density is given as

$$\rho = \rho_0 (1 - c_f \varphi) \tag{7}$$

with ρ_0 as the solid density and $c_f = \frac{\rho_0 - \rho_f}{\rho_0}$. The shear and bulk viscosity are given by the simple equations

$$\eta_s = \eta_{s0}(1 - \varphi) \tag{8}$$

and

$$\eta_b = \eta_{s0} \frac{1-\varphi}{\varphi} \tag{9}$$

where η_{s0} is the intrinsic shear viscosity of the matrix.

As in both equations (3) and (4) P is the fluid pressure, these equations can be merged to eliminate the pressure resulting in

$$\vec{v}_f - \vec{v}_s = -\frac{k_0 \varphi^{n-1}}{\eta_f} \left(\rho_0 c_f \vec{g}(1 - \varphi) + \frac{\partial \tau_{ij}}{\partial x_j} \right). \tag{10}$$

This equations states that the fluid separation flow i.e. melt segregation velocity) is driven by the buoyancy of the fluid with respect to the solid and the viscous stress in the matrix including compaction and decompaction.

Following Šrámek *et al*. (2007) the Stokes equation (3) can be rewritten by expressing the matrix velocity, $\vec{v}_s$, as the sum of the incompressible flow velocity, $\vec{v}_1$, and the irrotational (compaction) flow velocity, $\vec{v}_2$, as:

$$\vec{v}_s = \vec{v}_1 + \vec{v}_2 = \begin{pmatrix} \frac{\partial \psi}{\partial z} \\ -\frac{\partial \psi}{\partial x} \end{pmatrix} + \begin{pmatrix} \frac{\partial \chi}{\partial x} \\ \frac{\partial \chi}{\partial z} \end{pmatrix} \tag{11}$$

with ψ as stream function and χ as the irrotational velocity potential, given as the solution of the Poisson equation

$$\vec{\nabla}^2\chi = \vec{\nabla}\cdot\vec{v}_s. \tag{12}$$

The divergence term $\vec{\nabla}\cdot\vec{v_s}$ can be derived from eqs. 1 and 2 to give

$$\vec{\nabla}\cdot\vec{v}_s = -\vec{\nabla}\cdot\left[\varphi\left(\vec{v}_f - \vec{v}_s\right)\right]. \tag{13}$$

In the small fluid viscosity limit the viscous stresses within the fluid phase are neglected, resulting in a viscous stress tensor in the Stokes equation of the mixture (equ. 4), in which only the stresses in the solid phase are relevant. This is evident from the definition of the viscous stress tensor, which only contains matrix and not fluid viscosities. Melt viscosities of carbonatitic, basaltic or silicic wet or dry melts span a range from < 1 Pa s to extreme values up to 10^{14} Pa s (see the discussion in Schmeling et al., 2019), while effective viscosities of mafic or silicic partially molten rocks may range between 10^{20} Pa s and 10^{16} Pa s, depending on melt fraction, stress, and composition. Thus, in most circumstances the small fluid viscosity limit is justified.

In the limit of this small viscosity assumption, inserting the above solid velocity (11) into the viscous stress (6), this into the Stokes equation (4), and taking the curl of the x- and z equations the pressure is eliminated and one gets

$$\left(\frac{\partial^2}{\partial x^2} - \frac{\partial^2}{\partial z^2}\right)\left[\eta_s\left(\frac{\partial^2\psi}{\partial x^2} - \frac{\partial^2\psi}{\partial z^2}\right)\right] + 4\frac{\partial^2}{\partial x\partial z}\left[\eta_s\frac{\partial^2\psi}{\partial x\partial z}\right] = -g\frac{\partial\rho}{\partial x} + A(\chi) \tag{14}$$

with

$$A(\chi) = -2\frac{\partial^2}{\partial x\partial z}\left[\eta_s\left(\frac{\partial^2\chi}{\partial x^2} - \frac{\partial^2\chi}{\partial z^2}\right)\right] + 2\left(\frac{\partial^2}{\partial x^2} - \frac{\partial^2}{\partial z^2}\right)\left[\eta_s\frac{\partial^2\chi}{\partial x\partial z}\right] \tag{14a}$$

To describe the transition from solitary waves to diapirs it is useful to non-dimensionalize the equations. As scaling quantities we use the radius r of the anomaly, the reference viscosity η_0, and the scaling Stokes sphere velocity (e.g. Turcotte & Schubert, 1982) based on the maximum porosity of the porosity anomaly φ_{max}

$$v_{St} = \frac{\varphi_{max}\Delta\rho g r^2}{\eta_0} \tag{15}$$

resulting to the following non-dimensionalization where non-dimensional quantities are primed:

$$(x,z) = (x',z')\cdot r\,, \quad \vec{v}_{s,f} = \vec{v}_{s,f}{}'\cdot v_{St}, \quad t = t'\cdot\frac{r}{v_{St}}, \quad \left(\tau_{ij},P\right) = \left(\tau_{ij}{}',P'\right)\cdot\frac{\eta_0 v_{St}}{r},$$

$$(\eta_s,\eta_b) = (\eta_s{}',\eta_b{}')\cdot\eta_0, \quad (\psi,\chi) = (\psi',\chi')\cdot r v_{St} \tag{16}$$

We use the width corresponding to a $1/e$ drop of the initial perturbation as radius for the Stokes velocity. This is reasonable as the amount of melt in the perturbation is approximately equal to the amount of melt in a spheres cut with a sharp boundary of radius r, for what the Stokes equation is valid.

With these rules the Darcy equation (10) is given in non-dimensional form

$$\vec{v}_f{}' - \vec{v}_s{}' = -\frac{\varphi^{n-1}}{Rt}\left(\vec{e}_z\frac{(1-\varphi)}{\varphi_{max}} + \frac{\partial\tau_{ij}{}'}{\partial x_j{}'}\right) \tag{17}$$

where

$$Rt = \frac{\eta_f r^2}{\eta_0 k_0} \tag{18}$$

is the retention number based on the length scale of the anomaly and $\vec{e}_z$ is the unit vector in z-direction, and the momentum equation of the mixture (12) is given by

$$\left(\frac{\partial^2}{\partial x\prime^2} - \frac{\partial^2}{\partial z\prime^2}\right)\left[\eta_s{}'\left(\frac{\partial^2\psi\prime}{\partial x\prime^2} - \frac{\partial^2\psi\prime}{\partial z\prime^2}\right)\right] + 4\frac{\partial^2}{\partial x\prime\partial z\prime}\left[\eta_s{}'\frac{\partial^2\psi\prime}{\partial x\prime\partial z\prime}\right] = \frac{1}{\varphi_{max}}\frac{\partial\varphi}{\partial x\prime} + A'(\chi') \tag{19}$$

In the other equations (1), (2), (6), (11), (12), (13), and (14a) all quantities are simply replaced by their non-dimensional primed equivalents.

We now can compare the two limits, where segregation or two-phase flow dominates (solitary wave regime), and where fluid and solid rise together with the same velocity as partially molten bodies (batch melting), which we identify with the diapir regime. This can be done by comparing the characteristic segregation velocity within solitary waves, which scales as

$$v_{sgr} \approx \frac{k_0{\varphi_{max}}^{n-1}}{\eta_f}\left(\Delta\rho g(1-\varphi_{max}) - \frac{\partial\tau_{ij}}{\partial x_j}\right) = C\frac{k_0{\varphi_{max}}^{n-1}\Delta\rho g(1-\varphi_{max})}{\eta_f} \tag{20}$$

where C is of the order ½ for 2D solitary waves (Schmeling, 2000), with the characteristic Stokes sphere rising velocity given by (15). The ratio of these is given by

$$\frac{v_{sgr}}{v_{st}} = C\frac{{\varphi_{max}}^{n-2}(1-\varphi_{max})}{Rt} \tag{21}$$

Thus, *in the solitary wave limit*

$$\frac{Rt}{C{\varphi_{max}}^{n-2}(1-\varphi_{max})} \ll 1 \tag{22}$$

and Darcy's law (17) results in large segregation velocity, which scales as

$${v_{sgr}}' = C\frac{(1-\varphi_{max}){\varphi_{max}}^{n-1}}{Rt} \tag{23}$$

From equation (13) it follows that the irrotational part of the matrix velocity scales with

$$v_1 \approx -\varphi_{max}v_{sgr} \tag{24}$$

while the rotational part is given by (19): In that equation A' scales with χ', which, via equ (12) and (13), scale with v_{sgr}, i.e. with $\frac{1}{Rt}$. In other words, the second term on the RHS of (19) dominates for small Rt as the first term is of the order 1. Thus, the rotational matrix velocity has the same order as

the irrotational compaction velocity and serves to accommodate the compaction flow. In this limit the buoyancy term in equation (19), $\frac{1}{\varphi_{max}}\frac{\partial \varphi}{\partial x\prime}$, is of vanishing importance for the matrix velocity and the matrix velocity, $\vec{v}_1 + \vec{v}_2$, is of the order of $\varphi_{max} v_{sgr}$. In the small porosity limit, matrix velocities are negligible with respect to fluid velocities.

In the diapir limit,

$$\frac{Rt}{C{\varphi_{max}}^{n-2}(1-\varphi_{max})} \gg 1 \tag{25}$$

and equation (17) predict vanishing segregation velocities. As A' and χ' scale with $\frac{1}{Rt}$, both vanish in the diapir limit, no irrotational matrix velocity occurs and equ. (19) reduces to the classical biharmonic equation (i.e. Stokes equation) driven by melt buoyancy. Segregation velocities are negligible with respect to matrix velocities.

We will often refer to the compaction length, δ_c, which is a typical length scale used in two-phase flow problems (McKenzie, 1984). Of particular importance in our context, 2D porosity waves have half widths radii of the order of $3\delta_c$ to $5\delta_c$ (Simpson and Spiegelman, 2011). The compaction length is defined as:

$$\delta_c = \sqrt{\frac{\eta_b + \frac{4}{3}\eta_s}{\eta_f} k_\varphi} \tag{26}$$

The non-dimensional value $\delta_c' = \frac{\delta_c}{r}$ can be calculated using Rt with

$$\delta_c' = \sqrt{\frac{\eta_b' + \frac{4}{3}\eta_s'}{Rt} \varphi^n} \tag{27}$$

2.2 Model setup

The model consists of a $L' \times L'$ box with a background porosity, φ_0, of 0.5%. L' is the the non-dimensional side length of the box and equal to 20 times the initial radius of the perturbation. As initial condition a non-dimensional Gaussian wave porosity anomaly is placed at ${x_0}' = 10$ and ${z_0}' = 4$. It has the form of

$$\varphi = A \cdot \exp\left(-\left(\frac{x' - {x_0}'}{r'}\right)^2 - \left(\frac{z' - {z_0}'}{r'}\right)^2\right) \tag{28}$$

where A is the amplitude equal to 0.03 in our models and r' the non-dimensional width of the wave. r' in the model is always equal to 1, as it is used for non-dimensionalization. To vary the radius of the anomaly in terms of compaction lengths we change the retention number, which varies the compaction length. While the radius of an emerging solitary wave is always in the order of a few compaction lengths,

by varying Rt, the radius of the initial anomaly is varied between 1.5 and 100 times the compaction length to explore the parameter range in which diapirs might become dominant. The model box has always the same resolution, but the compaction length is differently resolved for each model. Even though this might lead to problems, as the compaction length should be always resolved equally, we are not able to do this, because our model series will inevitably lead to very small compaction lengths and keeping it equally resolved would require model resolutions we are not capable of performing. The numerical issues regarding this will be addressed later in this work.

At the top and the bottom, we prescribe an out- and inflow for both melt and solid, respectively, which is calculated analytically for the background porosity. This is necessary because we have a background melt fraction φ_0, that has a certain buoyancy which would lead to an accumulation of melt at the top of the model. We therefore calculate the segregation velocity of the background porosity φ_0 using equation (17) without the viscous stress term. The corresponding matrix velocity is calculated using the conservation of mass.

At the sides we use mirroring boundary conditions, which corresponds to a symmetry axis, where no horizontal flow is allowed. The permeability-porosity relation exponent in our models is always $n = 3$.

Our strategy is to vary the width of the initial porosity wave to cover the range from solitary waves to diapiric rise. Practically this is done by varying Rt and keep the non-dimensional radius constant. Here we give a small example:

For $Rt = 10^{-4}$ the initial perturbation, which has always a non-dimensional radius of $r' = 1$, has a dimensional radius of $r = 1.5 \cdot \delta_c$. With $Rt = 2.5 \cdot 10^{-3}$, the dimensional radius will be equal to $r = 10 \cdot \delta_c$, while r' is still equal to 1. Suppositious a solitary wave has always a similar radius in terms of compaction lengths, in the first case a solitary wave with $r_{sw} = 5 \cdot \delta_c$ will in our non-dimensionalization have a radius of $r'_{sw} = 2.5$. While in the second case the same wave will have a radius of $r'_{sw} = 0.5$. In a dimensional world this might correspond to enlarging the initial perturbation and keeping the compaction length constant or vice versa.

2.3 Numerical strategy

The above equations in non-dimensional form are solved by the finite differences code FDCON developed essentially by one of the authors (Schmeling). In the following, the non-dimensional versions of all equations are used. Starting from the prescribed initial condition for φ, and assuming $A'(\chi') = 0$ at time 0, the time loop is entered and the biharmonic equation (19) is solved for ψ' by Cholesky decomposition, from which $\vec{v}_1{}'$ is derived. Together with $\vec{v}_2{}'$ the resulting solid velocity is used to determine the viscous stress term in the segregation velocity equation (17). This equation and the melt mass equation (1) are solved iteratively with strong damping for φ and $\vec{v}_f{}' - \vec{v}_s{}'$ for the new time step using upwind and an implicit formulation of equ. (1). During this internal iteration these quantities are

used, via equ. (13), to give $\vec{\nabla} \cdot \vec{v}_s$, the divergence of the matrix velocity, which is needed in the viscous stress term (equ. 6). After convergence $\vec{\nabla} \cdot \vec{v}_s$ is used via equ. (12) to determine χ by LU-decomposition and then to get $\vec{v}_2{}'$. Now $A'(\chi')$ can be determined to be used on the RHS of equ (19). The procedure is then repeated upon entering the next time step.

Time steps are dynamically adjusted by the Courant criterion times 0.2 based on the fastest velocity, either melt or solid. We use a regular grid with 201 x 201 grid points.

3 Results

3.1 The transition from porosity wave to diapirism: Varying the initial wave radius

In this model series we vary the initial wave radius to cover the transition from porosity waves to diapirs. For small radii ($r \leq 10 \cdot \delta_c$) we can clearly see the emergence of solitary waves (Fig. 1 top row). $r = 1.5 \cdot \delta_c$ leads to a wave that is nearly the size of the initial perturbation. Even smaller radii would lead to bigger waves but with a smaller porosity amplitude as the melt needs to be conserved. For bigger radii the resulting solitary waves become smaller with respect to the initial size and lead to a focusing of melt. With an initial radius of $10 \cdot \delta_c$ the resulting wave has just a size of ~20% the initial wave size after it has risen half a box length.

We can compare the observed rising velocities of these solitary waves of Fig. 1 a to d with hypothetical Stokes velocities of an equivalent diapir based on equ. (15). While the dimensional Stokes velocity of a porosity anomaly is proportional to the amplitude of porosity and the square of the radius, the non-dimensional Stokes velocity is always equal to 1. In Fig. 2 this non-dimensional Stokes velocity is indicated by the dashed line with the value 1. The colored lines in Fig. 2 give 2D solitary wave velocities, given by Simpson & Spieglman (2011), normalized by the Stokes velocity corresponding to different initial perturbation radii. Inspection of Fig. 2 reveals that for the first 4 cases of Fig. 1a to d with radii smaller or equal $10 \cdot \delta_c$ the phase velocities are always larger than the Stokes velocity, i.e. the cases are in the solitary wave regime.

For greater radii (e.g. $r = 20 \cdot \delta_c$ or $30 \cdot \delta_c$, Fig. 1e or f, respectively) we see a focusing of melt in a narrow channel with a width of a few grid sizes. Inspection of Fig. 2 reveals that the solitary wave phase velocity of these cases is smaller than the Stokes velocity of the total porosity anomaly. We expect that the Stokes velocity of the non-circular porosity anomaly at later stages such as the stages shown in Fig. 1 is still of the order of the circular anomaly which approximately obeys equ. (15). Thus, the observed channel is no more the wake of a very small leading porosity wave, which is no more properly resolved by the numerical grid. Instead, we conjecture that these cases represent the transition to diapiric rise of the porosity anomaly, during which horizontal extensive stresses and strain rates within the upper, frontal part of the diapir lead to a channeling instability. Such channeling instabilities have been predicted in 1D by Stevenson (1989) and have been modelled without buoyancy by Richardson (1998)

in 2D. Golabek et al. (2008) obtained such channels in a partially molten mantle in front of sinking dense bodies. The channels were oriented radially away from the frontal hemisphere of the body, with the dominating channel pointing in the direction of the movement of the dense body. According to Stevenson (1989) the characteristic wavelength of such channels is expected to be of the order of $2\pi\delta_c$. In Fig. 1e and f the width of the observed channels is about $6-9\cdot\delta_c$, i.e. on the order of the characteristic wavelength. With a grid size of $2\cdot\delta_c$ and $3\cdot\delta_c$ for the cases shown in Fig. 1e and f the channels are close to but still above the resolution limit. In contrast to Golabek et al. (2008) the leading channel immediately dominates and is fed by buoyant melt out of the following porosity anomaly, no side channels evolve as in Golabek et al., (2008). This is probably due to their different compositional approach which prohibits such feeding. This channeling instability will be further discussed below.

For $r > 40\cdot\delta_c$ the channeling instability disappears, probably because it is below the resolution limit (grid size $< 4\cdot\delta_c$ for $r > 40\cdot\delta_c$) and we enter the diapir regime. In the diapir regime all perturbations evolve similar with a comparable velocity and in the same shape. In this diapir regime ($r > 40\cdot\delta_c$) Fig. 2 shows that the solitary wave velocities are at least one order of magnitude below the Stokes velocity of the diapir.

Summarizing Fig. 2, the comparison of Stokes and porosity wave velocities correlates nicely with the transition from diapirism to solitary waves shown in Fig. 1: For bigger radii the Stokes velocities are higher than the solitary wave velocity and the latter is therefore not the driving force of the ascending process and consequently not able to build up. For small radii the solitary wave velocity is clearly higher and therefore able to build up. Just by comparison of these curves, perturbations with $r > 20\cdot\delta_c$ should lead to diapirism while $r < 20\cdot\delta_c$ should lead to solitary waves.

3.2 Effects on the mass flux

It is important to study the partitioning between rising melt and solid mass fluxes in partially molten magmatic systems, because melts and solids are carriers of different chemical components. Within our Boussinesq approximation we may neglect the density differences between solid and melt. Then our models allow to evaluate vertical mass fluxes of solid or fluid by depicting the vertical velocity components multiplied with the melt or solid fractions, respectively:

$$\begin{aligned} q'_{sz} &= (1-\varphi)\cdot v'_{sz} \\ q'_{fz} &= \varphi\cdot v'_{fz}. \end{aligned} \tag{29}$$

Fig. 3 shows horizontal profiles through rising melt bodies at the vertical positions of maximum melt fraction.

The mass fluxes of solid and fluid are strongly affected by the change of the initial radius from the solitary wave regime to the diapiric regime. For $r = 1.5\cdot\delta_c$, where we observe a solitary wave, the fluid has its peak mass flux in the middle of the wave and the solid is going downwards, against the

phase velocity. In the center the fluid flux is more than 10 times higher than the solid. The net upward flow in the center is balanced by the matrix dominated downward flow outside the wave. For $r = 10 \cdot \delta_c$ the wave area is much smaller and the ratio between solid and fluid flux is around the order of one. Even though we observe a local minimum in the center of the wave for the solid flux it is not negative. However, the solid matrix around the wave is affected in a much greater area and, contrary to the case for $r = 1.5 \cdot \delta_c$, the rising net mass flux in and around the melt anomaly is dominated by the solid rather than melt flux.

For $r = 50 \cdot \delta_c$ and $r = 100 \cdot \delta_c$ the solid flux is significantly higher than the fluid flux also within the melt anomaly.

So far, we have based our discussion of the transition between solitary waves and diapirs on qualitative model observations. We now try to invoke a more quantitative criterion. In a horizontal line passing through the anomalies porosity maximum we define the total vertical mass flux of the rising magma body by $\int_{\varphi>\varphi_0}(q_f + q_s)dx$ where the integration is carried out only in the region of increased porosity $\varphi > \varphi_0$. This mass flux is partitioned between the fluid mass flux, $\int_{\varphi>\varphi_0} q_f dx$, and the solid mass flux, $\int_{\varphi>\varphi_0} q_s dx$. With these we define the partition coefficients

$$C_{soli} = \frac{\int_{\varphi>\varphi_0} q_f dx}{\int_{\varphi>\varphi_0}(q_f + q_s)dx} \tag{30}$$

and

$$C_{dia} = \frac{\int_{\varphi>\varphi_0} q_s dx}{\int_{\varphi>\varphi_0}(q_f + q_s)dx} \tag{31}$$

The sum $C_{soli} + C_{dia}$ is always 1 and if $C_{soli} > C_{dia}$ then the solitary wave proportion is dominant, while for $C_{soli} < C_{dia}$ diapirism is dominant. In Fig. 4a these partition coefficients for several initial radii are shown. In red are the partition coefficients calculated at a horizontal line at the height of maximum melt fraction. The blue markers are calculated for horizontal lines at all grid points below the maximum melt fraction as long as $\varphi \geq \frac{\varphi_{max}}{2}$. For $r = 1.5 \cdot \delta_c$, C_{soli} is equal to 1.5 and C_{dia} is equal to -0.5, i.e. we have a downward solid flux. With increasing radius C_{dia} increases until it changes its direction at $r = 4 \cdot \delta_c$. For even bigger radii C_{dia} increases further until it approaches 1 at approximately $r = 40 \cdot \delta_c$. C_{soli} changes so that the sum of both is always equal to 1. Even though diapirism is dominant for $r > 7.5 \cdot \delta_c$ we still observe a small solitary wave for $r = 10 \cdot \delta_c$ (c.f. Fig. 1) and the formation of channels until $r = 40 \cdot \delta_c$ where the melt segregation velocity $\overrightarrow{v_f}$ becomes slower than the matrix velocity $\overrightarrow{v_s}$. In Fig. 4b the ratio of maximum fluid velocity (i.e. $\overrightarrow{v_f}$) to absolute matrix velocity is shown. For small radii, where $C_{soli} \gg C_{dia}$, this ratio is approximately constant with a high value of

about 300. The absolute velocity maxima itself are not constant but decrease with the same rate until the switch of negative to positive matrix mass flux, where the absolute matrix velocity starts to increase, while the fluid velocity keeps decreasing. At this zero crossing we would expect a ratio of infinity, but with our models we are far enough away to not see this in the data. This switch from negative to positive mass flux was already observed by Scott (1988), but while he changed the viscosity ratio, we change the radius and keep the viscosity ratio constant. Both describe the transition from a two-phase limit towards the Stokes limit, but in our formulation, we are able to reach the Stokes limit while Scott (1988) is still in the two-phase flow regime. In the regime where a channel forms near the front of the porosity anomaly ($r = 20 \cdot \delta_c$ to $r = 40 \cdot \delta_c$) the ratio decreased from 20 to 2 (i.e. to $\overrightarrow{v_f} = \overrightarrow{v_s}$). In this regime, porous flow within the evolving channels is still very effective, and strongly exceeds the diapiric rising velocity. Above this point the channeling instability is no longer observed and clear diapirism can be observed. The calculated partition coefficients at lower elevations show that within the point of maximum melt fraction, C_{soli} is highest and decreases behind the ascending peak. Apparently, the fluid is locally able to build up a high porosity channel with segregating melt even though diapirism is dominant in the whole region. For small radii the partition coefficients vary strongest because the melt fraction decreases strongly behind the center of the wave.

Based on these observations the evolution of these models can be divided into 3 regimes: (1) In the solitary wave regime ($r \leq 7.5 \cdot \delta_c$) C_{soli} is larger than C_{dia} and the initial perturbation emerges into waves that have the properties of solitary waves and ascend with constant velocity and staying in shape. This regime can be further divided into 1a ($r < 4 \cdot \delta_c$) ,where the solid mass flux is negative, and 1b ($4 \cdot \delta_c < r \leq 7.5 \cdot \delta_c$), where the solid moves upwards with the melt. Waves in these regimes are very similar and differ only in the matrix flux.

In the transitional regime (2) ($7.5 \cdot \delta_c > r \geq 40 \cdot \delta_c$) C_{dia} is bigger than C_{soli} but either a small solitary wave may form near the front of a diapir ($r = 10 \cdot \delta_c$) or diapirs with leading high porosity channels can be observed. Even though diapiric ascend is dominant, melt is locally able to focus into channels because the fluid is still faster than the matrix. This leads to a small peak of high porosity at the front of the channel followed by a broader area ascending as diapir. We may call this regime "porosity wave or diapir induced melt focusing and channeling".

In regime (3) ($r > 40 \cdot \delta_c$) the segregation velocity is smaller than the matrix velocity (i.e. $\frac{\max(v_f)}{\max(v_s)} \leq 2$) and the fluid is therefore no longer able to separate fast enough to build up a solitary wave or a focusing channel. Dominated by solid mass flux a well-developed diapir will ascend.

3.3 Numerical Issues

In Fig. 5 a model with an initial perturbation radius of $r = 60 \cdot \delta_c$ is shown in three different model resolutions. While for the lowest resolution (Fig. 5a) a diapir can be observed, an increased resolution

of 301x301 shows some localization of melt at the top of the diapir. With the highest resolution the grid size is equal to approximately two times the compaction length, and a strongly focused channel in front of the initial perturbation builds up, and two weak side lobes appear at a distance of about $28 \cdot \delta_c$ on each side of the channel. Inspecting the wavelength dependence of channeling instabilities (Stevenson, 1989), this is about four times the wavelength at which the growth curve approaches its maximum value and remains constant for smaller wavelengths. Richardson (1998) investigated the melt channeling instability and found that it is grid space dependent: "when the grid spacing is of the order of the compaction length", as in our case in Fig. 5c, "the instability locks onto a small multiple of the grid spacing, and so the solution is affected by the discretization for the numerical calculation" In the cases of Fig. 5a and b the grid spacing is larger than the compaction length prohibiting the evolution of the channeling instability, while in case of Fig. 5c Richardson's (1998) criterion is met and channeling occurs.

With this perception it is interesting to reevaluate the model series in Fig. 1. The models within the diapir-regime and $r > 40 \cdot \delta_c$ do not show any sign of developing a frontal channel. This may be explained by the coarse resolution, because the compaction lengths are significantly less than the grid size. We expect, that if the grid resolution would be increased appropriately as in the resolution test in Fig. (5), also these models would show frontal channel(s) on the scale of small multiple of the grid spacing. Because of practical reasons we did not test this conjecture for other r's than that in Fig. 5.

4 Discussion

4.1 The channeling instability

In this chapter we compare the observed formation of channels at the top of some of the porosity anomalies with the growth rate of the channeling instability analytically derived by Stevenson (1989). For wavelengths of the order of $2\pi\delta_c$ and smaller the growth rate of channel like porosity perturbations oriented perpendicular to the direction of a background extensional strain rate $\dot{e}_0$ is given by

$$\alpha_0 = \frac{2\eta_s a_\eta \dot{e}_0}{\left(\eta_b + \frac{4}{3}\eta_s\right)} \tag{32}$$

where a_η gives the porosity dependence of the shear viscosity

$$a_\eta = -\frac{d \ln(\eta_s)}{d\varphi} \tag{33}$$

Using our rheology laws (8) and (9) we arrive at

$$\alpha_0 = \frac{2\varphi \dot{e}_0}{(1-\varphi^2)} \tag{34}$$

We non-dimensionalize the growth rate by using our scaling velocity and scaling length, i.e. $\frac{v_{St}}{r}$. This quantity happens to scale with the characteristic strain rate near the top of the circular porosity wave, i.e. with $\dot{e}_0$. Thus, the non-dimensional channeling growth rate reduces to

$$\alpha_0{}' = \frac{2\varphi}{(1-\varphi^2)} \tag{35}$$

Inspecting the time-dependence of our high resolution model with $r = 60 \cdot \delta_c$ (Fig. 5c) which show focusing of fluid within a narrow channel at the top of the porosity anomaly allows to estimate the growth rate of the porosity increase within the channel. If at some early stage $t_0{}'$ of the channel evolution the amplitude is $A_0 = \varphi_{channel} - \varphi_{ambient}$ and the amplitude grows exponentially as $A(t') = A_0 exp(\alpha_0{}'(t' - t_0{}'))$ we can determine $\alpha_0{}'$ by

$$\alpha_0{}' = ln\left(\frac{A}{A_0}\right)/(t - t_0) \tag{36}$$

These experimentally determined $\alpha_0{}'$ range between 0.5 and 0.72 with a mean of 0.60, which is larger than the analytical $\alpha_0{}'$ derived from equ. (35) by a factor of about 7. We explain this higher experimental growth rate by a) circular geometry, according to which the central channel grows faster than any other channels. Actually, in Fig. 5c this is visible: beside the central channel two weak side lobes appear, and it can be conjectured that the main channel has grown faster by about a factor 3 on the expense of these side channels. b) In Stevenson's (1989) analysis buoyancy has not been included. In our case the fluid within the channel rises and accumulates in the upper part. If we would redistribute that fluid along the whole channel, the amplitude $A(t)$ would be smaller, perhaps by a factor 2. Altogether, taking these two effects into account, the agreement between the observed growth of the channeling instability and the analytical growth rate can be regarded as reasonably good. This justifies our interpretation of these channels resulting from this instability and being roughly resolved when the grid size is of the order of the compaction length.

4.2. Application to nature

While in our models the perturbation size in terms of compaction lengths was systematically varied but kept constant within in each model, our results might also be applicable to natural cases in which the compaction length varies vertically. In the case of compaction length decreasing with ascent a porosity anomaly might start rising as a solitary wave but then passes through the transition towards diapiric rise. In this case the solitary wave would most certainly enter the regime 2 characterized by strong focusing or channeling followed by a bigger perturbation. A decreasing compaction length could be accomplished by decreasing the matrix viscosity or the permeability, or by increasing the fluid viscosity. Decreasing matrix viscosity might be for example explainable by local heterogeneities, temperature anomalies for example due to secondary convective overturns in the asthenosphere or by a vertical gradient of water content, which may be the result of melt segregation aided volatile enrichment at shallow depths in

magmatic systems. This could lead to the propagation of magma-filled cracks (Rubin, 1995) as already pointed out in Connolly & Podladchikov (1998). The latter authors have looked at the effects of rheology on compaction-driven fluid flow and came to similar results for an upward weakening scenario. But this upward weakening might not be strong enough to lead to the focusing needed for the nucleation of dykes. The decrease of permeability due to decrease in background porosity might be an alternative explanation. In the hypothetic case of a porosity wave reaching the top of a magma chamber, the background porosity might decrease which would most certainly lead to focusing, because the compaction length will decrease, and eventually, when reaching melt free rocks, the melt rich fingers may stall as in our models at $r > 50 \cdot \delta_c$ and the rising melt will accumulate and enter the pure diapirism regime. But if the focusing is strong enough and the fluid pressure high enough this scenario could alternatively be a good explanation for the nucleation of dykes. Indeed, if the initiation of dyking is induced by melt channeling instabilities (Stevenson, 1989), our models constrain the minimum size for focused melt anomalies, namely a few compaction lengths. As discussed above, for a partially molten region subject to horizontal extensive stresses Stevenson (1989) determined the growth rate of a channeling instability and found that it reaches a flat maximum plateau for wavelengths smaller than the order of the compaction length. Thus, at the top of our porous diapirs the conditions for melt channeling and subsequent dyking may well be met. As discussed above due to limited resolution in our models we are not able to test this combination of diapiric rise and subsequent channeling on the sub-compaction length scale, however, our resolution test (Fig. 5) is a strong indication for this mechanism.

4.3. Other issues

The introduced partition coefficients help distinguish between a solitary wave and diapirism but there is more information needed, i.e. the matrix and fluid velocity, to really distinguish between the three regimes. For some cases focusing into solitary waves or channels can be observed despite diapirism being dominant. Not until the segregation velocity becomes slower than the matrix, pure diapirism can be observed. These regimes might be not directly applicable to different models e.g. with different amplitudes, rheology laws, permeability laws or background porosities, but their well-defined existence shows that they should exist in generality and the models shown here give an order of magnitude for which perturbation to compaction length ratios one needs to be careful.

The used equation for the Stokes velocity is valid for a sphere and not an infinite long cylinder like the initial perturbation in our 2D model. But still, the velocities fit quite nicely to the observed model velocities. There is no analytic solution for an infinite long cylinder in an infinite medium, but only the solution of a cylinder inside a cylinder with finite radius, where the ratio of both cylinders has some influence on the velocity. For the size of the initial cylindrical wave in a lager cylinder of characteristic size of our model box this solution is nearly identical to the solution of a sphere and therefore it doesn't make sense to use the mathematically more complex solution of a cylinder.

5 Conclusion

This work shows that, depending on the extent of a partially molten region within the earth, the resulting ascent of melt may not only occur by solitary waves or by diapirs, but by an intermediate new mechanism which we call "porosity wave or diapir induced melt focusing and channeling". Depending on the ratio of the melt anomalies size to the compaction length, quantitatively we can classify the ascent behavior into three different regimes using mass flux and velocity of matrix and melt: (1) Solitary wave a and b, (2) porosity wave or diapir induced melt focusing and channeling and (3) diapirism. In regime 1a the matrix sinks with respect to the rising melt, in 1b also the matrix rises, but very slowly. On first order these regimes can be explained by comparing Stokes velocity of the rising perturbation with the solitary waves phase velocity. If the Stokes velocity is higher a diapir will evolve, if lower, a solitary wave will evolve. But even if the Stokes velocity is higher, melt channeling instabilities might be able to focus melt locally within the rising diapiric plume into a frontal channel. These focused channels have a scale of the order of a few compaction lengths. Not until the segregation velocity becomes smaller than the matrix velocity, solitary waves are no longer able to evolve.

Especially in the second regime numerical resolution plays an important role as the compaction length might be no longer resolved properly. Hence it should be generally important for two-phase flow models to inspect the size of partially molten areas with respect to the compaction length, to decide whether possible solitary waves or channeling instabilities are resolved or not.

Code availability

The used finite difference code, FDCON, is available on request.

Author Contribution

Janik Dohmen wrote this article and carried out all models shown here. Harro Schmeling helped preparing this article and had the idea for this project.

References

Barcilon, V., & Lovera, O. M.: Solitary waves in magma dynamics. *Journal of Fluid Mechanics*, *204*(1989), 121–133. https://doi.org/10.1017/S0022112089001680, 1989.

Bittner, D., & Schmeling, H.: Numerical modelling of melting processes and induced diapirism in the lower crust. *Geophysical Journal International*, *123*(1), 59-70, 1995.

Connolly, J. A. D.: Devolatilization-generated fluid pressure and deformation-propagated fluid flow during prograde regional metamorphism. *Journal of Geophysical Research: Solid Earth*, *102*(B8), 18149-18173, 1997.

Connolly, J. A. D., & Podladchikov, Y. Y.: Compaction-driven fluid flow in viscoelastic rock. *Geodinamica Acta*, *11*(2–3), 55–84. https://doi.org/10.1080/09853111.1998.11105311, 1998.

Connolly, J. A. D., & Podladchikov, Y. Y.: A hydromechanical model for lower crustal fluid flow. In *Metasomatism and the chemical transformation of rock* (pp. 599-658). Springer, Berlin, Heidelberg, 2013.

Connolly, J. A. D., & Podladchikov, Y. Y.: An analytical solution for solitary porosity waves: Dynamic permeability and fluidization of nonlinear viscous and viscoplastic rock. *Geofluids*, *15*(1–2), 269–292. https://doi.org/10.1111/gfl.12110, 2015.

Dohmen, J., Schmeling, H., & Kruse, J. P.: The effect of effective rock viscosity on 2-D magmatic porosity waves. *Solid Earth*, *10*(6), 2103-2113, 2019.

Golabek, G. J., Schmeling, H., & Tackley, P. J. (2008). Earth's core formation aided by flow channelling instabilities induced by iron diapirs. *Earth and Planetary Science Letters*, *271*(1-4), 24-33.

Griffiths, R. W.: The differing effects of compositional and thermal buoyancies on the evolution of mantle diapirs. *Physics of the earth and planetary interiors*, *43*(4), 261-273, 1986.

Jordan, J. S., Hesse, M. A., & Rudge, J. F.: On mass transport in porosity waves. *Earth and Planetary Science Letters*, *485*, 65–78. https://doi.org/10.1016/j.epsl.2017.12.024, 2018.

McKenzie, D.: The generation and compaction of partially molten rock. *Journal of Petrology*, *25*(3), 713–765. https://doi.org/10.1093/petrology/25.3.713, 1984.

Omlin, S., Malvoisin, B., & Podladchikov, Y. Y.: Pore Fluid Extraction by Reactive Solitary Waves in 3-D. *Geophysical Research Letters*, *44*(18), 9267–9275. https://doi.org/10.1002/2017GL074293, 2017.

Richard, G. C., Kanjilal, S., & Schmeling, H. (2012). Solitary-waves in geophysical two-phase viscous media: A semi-analytical solution. *Physics of the Earth and Planetary Interiors*, *198–199*, 61–66. https://doi.org/10.1016/j.pepi.2012.03.001

Richardson, C. N.: Melt flow in a variable viscosity matrix. *Geophysical Research Letters*, *25*(7), 1099-1102, 1998.

Rubin, A. M.: Propagation of magma-filled cracks. *Annual Review of Earth and Planetary Sciences*, 287–336, 1995.

Schmeling, H.: Partial melting and melt segregation in a convecting mantle. In *Physics and Chemistry of Partially Molten Rocks*. Springer, 2000.

Schmeling, H., Marquart, G., Weinberg, R., & Wallner, H.: Modelling melting and melt segregation by two-phase flow: New insights into the dynamics of magmatic systems in the continental crust. *Geophysical Journal International*, *217*(1), 422–450. https://doi.org/10.1093/gji/ggz029, 2019.

Scott, D. R.: The competition between percolation and circulation in a deformable porous medium. *Journal Of Geophysical Research*, *93*(B6), 6451–6462. https://doi.org/10.1029/JB093iB06p06451, 1988

Scott, D. R., & Stevenson, D. J.: Magma solitons. *Geophysical Research Letters*, *11*(11), 1161–1164, 1984.

Simpson, G., & Spiegelman, M.: Solitary wave benchmarks in magma dynamics. *Journal of Scientific Computing*, *49*(3), 268–290. https://doi.org/10.1007/s10915-011-9461-y, 2011.

Spiegelman, M.: Physics of Melt Extraction: Theory, Implications and Applications. *Philosophical Transactions of the Royal Society A: Mathematical, Physical and Engineering Sciences*, *342*(1663), 23–41. https://doi.org/10.1098/rsta.1993.0002, 1993.

Spiegelman, M.: Flow in deformable porous media. Part 2 Numerical analysis - the relationship between shock waves and solitary waves. *J. Fluid Mech.*, *247*, 39–63. https://doi.org/10.1017/S0022112093000370, 1993.

Spiegelman, M., & McKenzie, D.: Simple 2-D models for melt extraction at mid-ocean ridges and island arcs. *Earth and Planetary Science Letters*, *83*(1-4), 137-152, 1987.

Šrámek, O., Ricard, Y., & Bercovici, D.: Simultaneous melting and compaction in deformable two-phase media. *Geophysical Journal International*, *168*(3), 964–982. https://doi.org/10.1111/j.1365-246X.2006.03269.x, 2007.

Stevenson, D. J.: Spontaneous small-scale melt segregation in partial melts undergoing deformation. *Geophysical Research Letters*, *16*(9), 1067-1070, 1989.

Turcotte, D. L., & Schubert, G.,. *Geodynamics*. Cambridge university press., 1982.

Watson, S., & Spiegelman, M.: Geochemical Effects of Magmatic Solitary Waves—I. Numerical Results. *Geophysical Journal International*, *117*(2), 284–295. https://doi.org/10.1111/j.1365-246X.1994.tb03932.x, 1994.

Wiggins, C., & Spiegelman, M.: Magma migration and magmatic solitary waves in 3D. *Geophysical Research Letters*, *22*(10), 1289–1292. https://doi.org/10.1029/95GL00269, 1995.

Collins, W. J.: Polydiapirism of the Archean Mount Edgar Batholith, Pilbara Block, Western Australia. *Precambrian Research*, *43*(1-2), 41-62, 1989.

Yarushina, V. M., Podladchikov, Y. Y., & Connolly, J. A. D.: (De)compaction waves in porous viscoelastoplastic media: Solitary porosity waves. *Journal of Geophysical Research: Solid Earth*, 1–20. https://doi.org/10.1002/2014JB011260.Received, 2015.

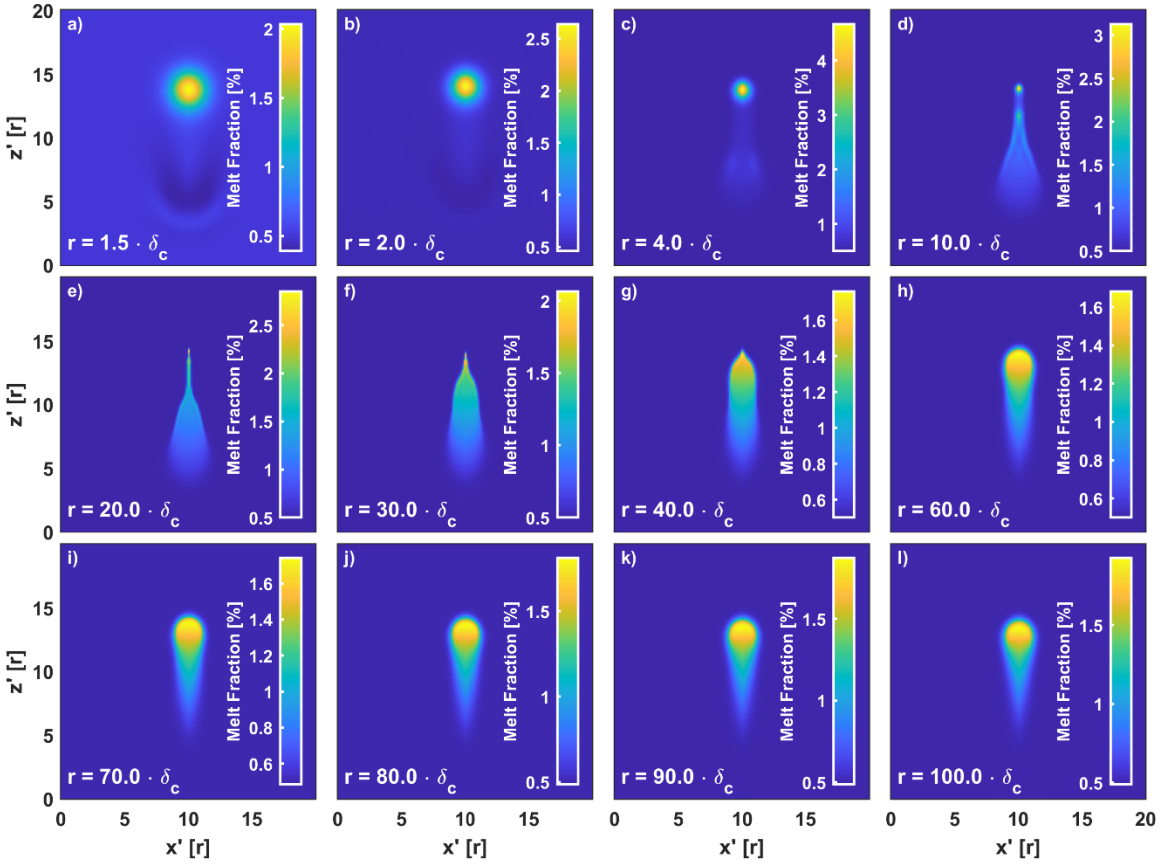

Fig. 1: Resulting melt fraction fields after the maximum melt fraction in the model has reached 70% of the boxes height for different initial perturbation sizes. The surface color gives the melt fraction in percent. The initial perturbation radius of the model is given in white in terms of compaction lengths.

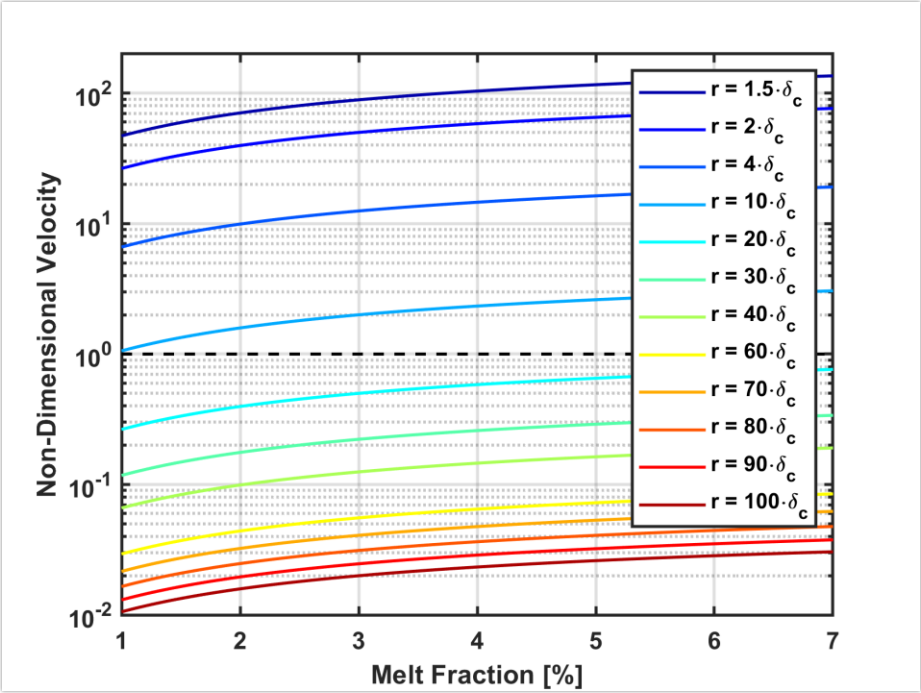

Fig. 2: The dashed line marks the velocity of the Stokes sphere ($v' = 1$). The colored lines show the velocity of a 2D solitary wave, calculated semi-analytically by Simpson & Spiegelman (2011), in our non-dimensionalization, based on the radii shown in the legend.

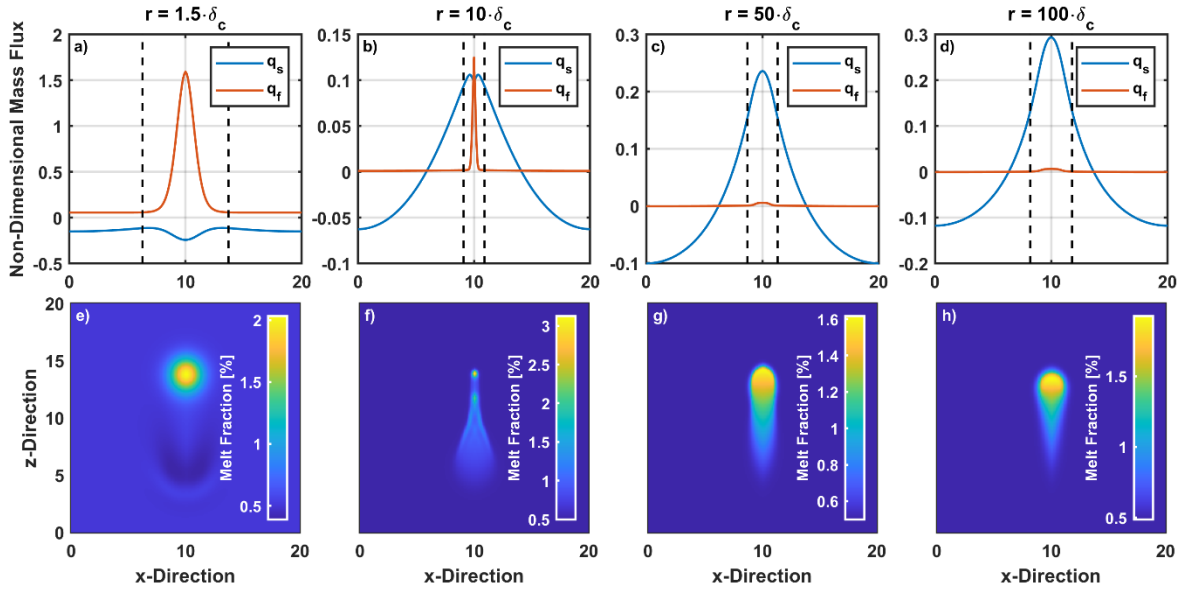

Fig. 3: The upper row gives the solid and fluid mass fluxes of a horizontal line cutting through the maximum melt fraction of the model after it has reached 70% of the models height for different initial perturbation radii. The bottom row gives the corresponding melt porosity fields. All quantities shown are non-dimensional.

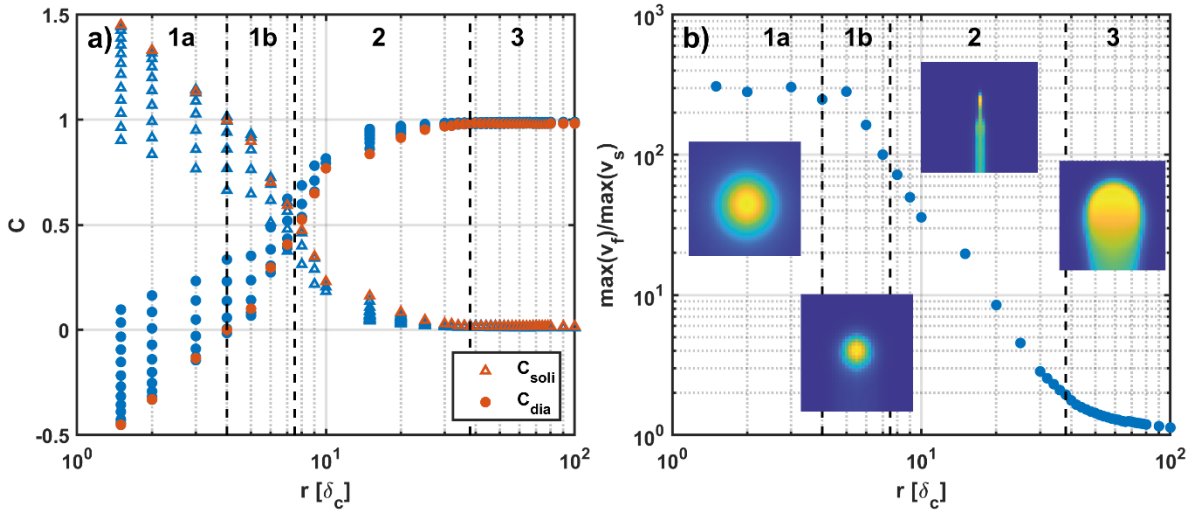

Fig. 4: a) The graph shows the solitary wave and diapir partition coefficients for several initial perturbation radii. The red marker gives the coefficients calculated on a horizontal line at the height of maximum melt fraction. All blue dots give the coefficients calculated at all grid points below the maximum melt fraction as long as at these horizontal lines maximum melt fraction is higher than half the model's maximum. The dashed lines are the borders of the regimes. Figure b) shows the ratio of maximum fluid velocity to maximum solid velocity in the whole model. The small pictures show typical melt fraction perturbations for each regime. The pictures are from models with an initial perturbation radius of 2, 6, 20 and 60 times the compaction length from left to right.

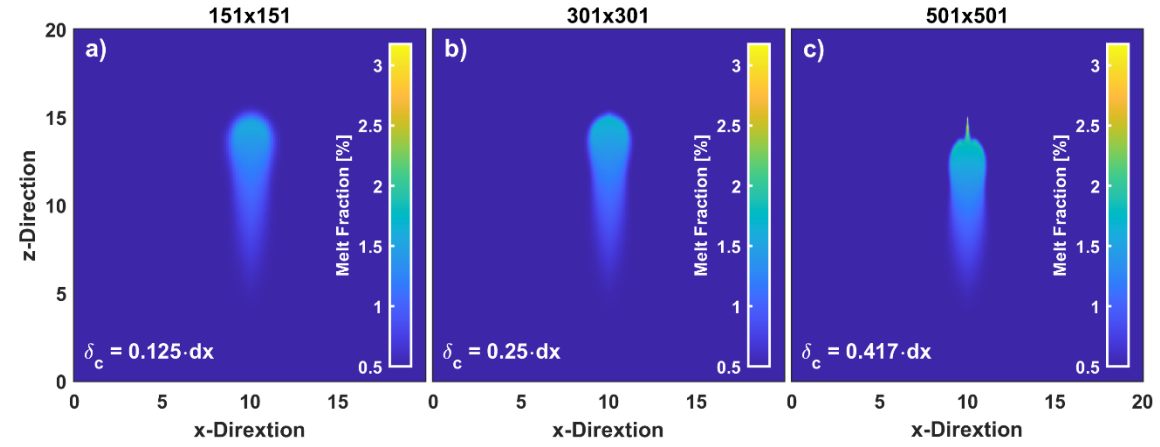

Fig. 5: All three figures show a model with an initial perturbation radius of 60 times the compaction length but with different resolutions: a) 151x151, b) 301x301, c) 501x501. In the lower left corner in each figure the size of the compaction length in terms of grid length is given.